Theoretical Prediction and Direct Observation of the 9*R* Structure in Ag

F. Ernst, M. W. Finnis, D. Hofmann, T. Muschik, U. Schönberger, and U. Wolf
Max-Planck-Institut für Metallforschung, Institut für Werkstoffwissenschaft, Seestrasse 92, 7000 Stuttgart 1, Germany

M. Methfessel
Fritz-Haber-Institut der Max-Planck-Gesellschaft, Faradayweg 4-6, 1000 Berlin 33, Germany
(Received 13 April 1992)

Molecular-dynamics simulations of the $\Sigma3\langle110\rangle(211)$ twin boundary in Ag predict a thin (1 nm) boundary phase of the 9*R* (α-Sm) structure. High-resolution electron microscopy shows the presence of the predicted structure. We also calculate the energy *ab initio* for several hypothetical structures of Cu and Ag. Low energies of the 9*R* structure and other polytypes, low experimental stacking-fault energies, and the hcp-fcc energy difference are correlated and explained in terms of an effective nearest-neighbor Ising interaction.

PACS numbers: 61.16.Di, 61.70.Ng, 68.35.Bs

It has been recognized for some time that the 9*R* polytype or α-Sm structure occurs as a martensitic product in a number of alloys [1–7] and compounds [8–10]. In pure metals, besides in Sm itself, the structure has been seen in quenched, ultrafine Co particles [11], in Cu precipitates in α-Fe [12], and in our own work on Cu and Ag twin boundaries to be reported. Furthermore, the 9*R* structure has received increasing attention recently from the physics community since it was identified by Overhauser [13] from neutron scattering data [14] as a stable structure of Li below 75 K. Subsequent work by Smith and others confirmed that there is a 9*R* phase, albeit heavily faulted, in Li below 75 K [15] and also in Na below 35 K [16]. The evidence that it exists at all in K appears to be weaker [16,17]. From a theoretical point of view first-principles calculations for metallic hydrogen have shown [18] that, among several candidate structures, the 9*R* is the most stable.

We report here the first observation of the 9*R* structure in pure Ag. It occurs in a rather special situation, namely, at a $\Sigma3(211)$ twin boundary, where a thin (1 nm) layer of the phase appears as a means to ease the reversal of the stacking sequence *ABC*... to *CBA*... from grain to grain. Its structure is appropriate for this purpose since it can be thought of as fcc with a stacking fault on every third close-packed plane. However, to occur at the boundary it is necessary that 9*R* be only slightly higher in energy than fcc, and as we shall show this is enabled by the low stacking-fault energy of Ag. The boundary structure was predicted by computer simulation, as described below. It has also been predicted and found in Cu [19]. Evidence has been published that it appears in Au [20], although it was not recognized at the time as such. Our direct experimental evidence for the structure was obtained by high-resolution transmission electron microscopy (HRTEM). We have also made first-principles total-energy calculations for polytypes and obtained stacking-fault energies which support our interpretation.

To understand the geometry of the 9*R* and other polytype structures it is helpful to note that the possible stacking sequences of close-packed planes are isomorphic to the Ising model. This is a useful way to think about polytypes [21–23]. The familiar notation *ABCABC*... for the stacking sequence in fcc, for example, obscures the fact that each close-packed plane has the same translation with respect to the one below. In the Ising model, fcc is represented by $[\downarrow]$. The arrow denotes one of the two possible translations and the square brackets contain one repeat unit. The hcp structure is the "antiferromagnetic" state $[\downarrow\uparrow]$ and the 9*R* structure is $[\downarrow\uparrow\uparrow]$. This representation exposes the fact that 9*R* is the third simplest way to stack close-packed planes of hard spheres, an observation which may make the varied occurrences of 9*R* in nature less mysterious. The next simplest structures in this sequence have repeat cells of four spins; these are $[\downarrow\downarrow\uparrow\uparrow]$ and $[\downarrow\downarrow\downarrow\uparrow]$, which are referred to as 4*H* and 12*R*, respectively. If we consider nonperiodic structures, the intrinsic stacking fault is $\ldots\downarrow\downarrow\uparrow\downarrow\downarrow\ldots$, the extrinsic stacking fault is $\ldots\downarrow\downarrow\uparrow\uparrow\downarrow\downarrow\ldots$, and the coherent $\Sigma3$ twin boundary is $\ldots\downarrow\downarrow\downarrow\uparrow\uparrow\uparrow\ldots$.

Molecular-dynamics simulations (MD) of the $\Sigma3(211)$ twin boundary in Ag have been performed using an empirical *N*-body potential [24]. A slab containing the boundary was constructed with periodic boundary conditions in the boundary plane. The boundary was 15 nm long in $\langle\bar{1}11\rangle$ and four atomic layers wide in $\langle110\rangle$, and the whole slab contained 9280 atoms. It was equilibrated at 500 K for 20 ps and then quenched to less than 1 K in order to examine the equilibrium structure. The resulting structure is almost identical to that obtained for Cu by static relaxation [19]. A piece of the relaxed Ag boundary is shown in Fig. 1. The atomic positions are projected in $\langle110\rangle$. The black or white color indicates to which of two adjacent (220) planes each atom belongs. The boundary is characterized by a thin slab of the 9*R* structure. It is separated from fcc on one side by kite-shaped structural units. The inclination of the 9*R* structure to the kites enables a good atomic matching on this side.

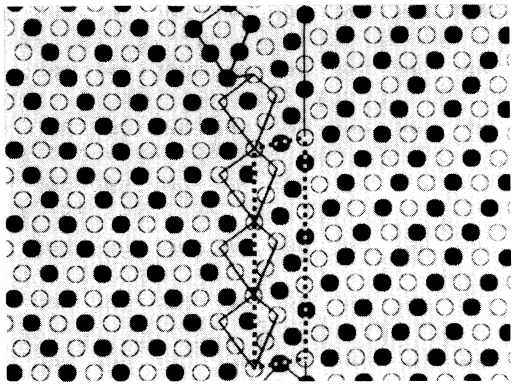

FIG. 1. A piece of the grain boundary in Ag simulated with molecular dynamics after annealing at 500 K for 20 ps followed by quenching.

On the other side the $9R$-fcc interface can be described as a low-angle boundary of partial dislocations, and this is also a relatively well-coordinated, low-energy structure. Near the edge of the figure is a monatomic step in the boundary. Such steps formed frequently during the dynamic simulation because they involve only slight atomic rearrangement, indicating that these boundaries are very mobile. From our previous static studies on Au [20] and Cu [19] and from the experimental observations, we expect that the formation of approximately 8° facets from such steps is energetically slightly favored, although like other reorientations this is likely to be suppressed in MD by the periodic boundary conditions.

For the microscopy, diffusion-bonded bicrystals [25] of 99.9998% Ag were annealed for 15 h at 1070 K to equilibrate the grain-boundary structure. The TEM specimens were prepared from these bicrystals by standard techniques, including ion-beam milling. The specimens were investigated in a JEM 4000EX (Jeol). Operating at 400 keV, this instrument reaches a point resolution of 0.175 nm. Edge-on images of the grain boundary viewed along ⟨110⟩ were recorded near the first passband. The sample thickness in the area of interest was determined by tilting the specimen and correlating the projected width of the boundary with the tilt angle. Experimental images were digitized using a diode-array camera with a dynamic range of 16 bits. The images contain long sections with a periodic structure. In Fig. 2(a) an image of one period is shown.

From this lattice image a best estimate of the x-y coordinates of atomic columns was obtained by a local correlation technique, details of which will be published elsewhere. The technique is justified as long as the conditions for application of the column approximation [26] are fulfilled. The resulting atomic positions are shown as black and white circles in Fig. 2(c). The black and white shading is not an experimental distinction: It represents our assignment of atomic positions to the two types of

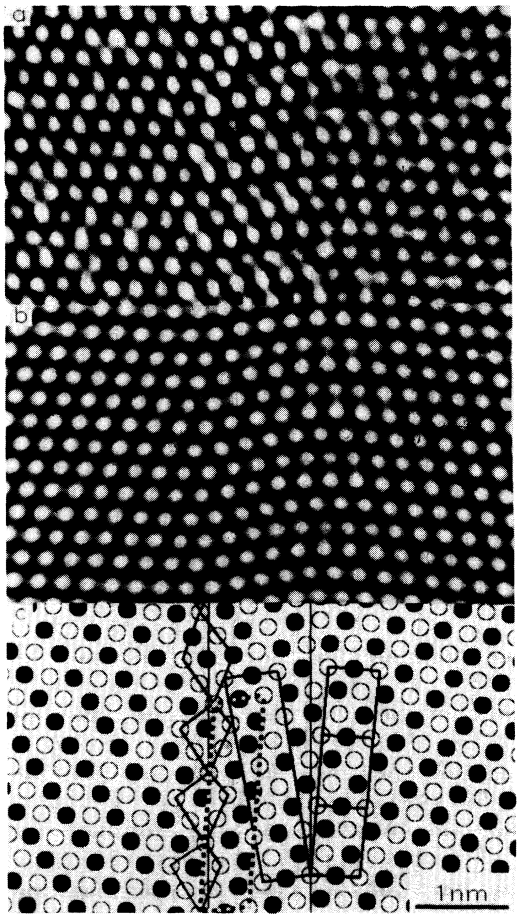

FIG. 2. The (a) observed and (b) simulated HRTEM images of the grain boundary in Ag. (c) The atomic coordinates (x,y) extracted from (a) and used for the simulation (b). The black and white shading is our assignment of atoms to one of the two (220) planes in the z direction.

(220) planes, based on a comparison with Fig. 1. We note that the two crystals are actually tilted by 3.1° about ⟨110⟩ compared to the perfect twin orientation.

The coherent imaging process of HRTEM can lead to artifacts in the image. In order to verify the structure obtained by the local correlation procedure, the atomic coordinates of Fig. 2(c) were used as input data for an image simulation [27] using the multislice method. The appropriate defocus value has been found by interpretation of the diffractogram of an amorphous region in the experimental negative. Figure 2(b) represents the simulated image, which matches the experimental one well. The experimental structure in Fig. 2 contains a thin slab of $9R$ between the two fcc crystals, in accord with the MD prediction.

In Fig. 2(c) we have indicated two alternative nonprimitive $9R$ unit cells. The dashed cell is directly comparable to that in Fig. 1. A rectangular $9R$ cell is also marked, the full symmetry of which would be rhom-

bohedral. In this cell the stacking sequence is most easily compared with fcc, a neighboring cell of which is outlined. At the left side of the boundary, besides the kite units which were also present in the MD simulations, we see a rhombus unit. This represents at once a microfacet and the core of a secondary dislocation. It introduces a fault in the $9R$ stacking sequence. From the lattice geometry, we have determined that the array of these rhombus units exactly accommodates the 3.1° misorientation to $\Sigma 3$. The resulting mean boundary plane lies on (17,9,9). We also note that the experimental boundary is tilted by several degrees away from the (211) plane of either crystal, thereby placing the low-angle $9R$-fcc interface symmetrically with respect to close-packed (111) planes on either side of it. The cause of this tilting has been identified. In the original (211) orientation, the $9R$ close-packed planes would have been slightly closer together than their bulk equilibrium spacing, causing an internal compressive stress. The tilting of the interface reestablishes the equilibrium interplanar spacing and relieves the stress. Finally we note that the width of the untilted boundary from the MD simulations is somewhat smaller than the experimental width. Static simulations of a ready-tilted boundary in Cu [19] showed that the tilting gives rise to exactly such a wider $9R$ region.

We now turn to our *ab initio* total-energy calculations. The Ising description also helps us here because it expresses the energy of stacking sequences simply in terms of nearest-neighbor, next-nearest-neighbor, etc., pairwise interactions. The applicability of the Ising description to a similar situation was demonstrated by Denteneer and Soler [28], who calculated the stacking-fault energies in Al. Here, we use *ab initio* calculations to obtain total energies for several stacking sequences of Cu and Ag. From these the pairwise couplings J_n can be deduced and the reason for the low energy of the $9R$ structure can be understood.

As the calculational procedure we used a frozen-potential technique (the force theorem) [29,30] based on the linear combination of atomic orbitals method in the atomic sphere approximation (LMTO-ASA) [31,32] as used by Skriver [33] to calculate fcc-hcp-bcc energy differences in the transition metals. The potential for each structure was constructed by placing the self-consistent reference ASA potential (here obtained from fcc) at each site. To first order, the differences of the single-particle eigenvalue sums then equal the differences of the self-consistent total energies, including non-ASA terms which are commonly thought to be outside the scope of the LMTO-ASA method. We used a minimal basis set of s, p, and d functions, combined correction terms, and up to 1000 k points in the irreducible wedge of the Brillouin zone to ensure convergence to within 0.01 mRy/atom. Table I shows the results, including the deduced Ising couplings J_1 to J_3. A central conclusion is that J_1 dominates the other couplings, even more than in Al [28]. The energy of the $9R$ structure relative to fcc is then simply given by a superposition of stacking-fault energies, just as in the empirical potential model we used for the MD simulations. This traces the competitiveness of the $9R$ structure to the low stacking-fault energies of the noble metals.

TABLE I. Structural energy differences for polytypes relative to fcc calculated with the force theorem. The second number is the value obtained directly from the hcp-fcc difference by assuming only J_1 coupling. Units are mRy/atom except the intrinsic stacking-fault energy γ_{int} which is in mJ m^{-2}. Experimentally estimated stacking-fault energies [35] are in parentheses. The three J values shown were obtained from the first three structural energy differences, using the expressions given in column 2.

		Cu	Ag
hcp	$2(J_1+J_3\ldots)$	0.79	0.43
$9R$	$\frac{4}{3}(J_1+J_2+\cdots)$	0.50, 0.53	0.28, 0.29
$4H$	$J_1+2J_2+J_3+\cdots$	0.41, 0.40	0.22, 0.22
$12R$	$J_1+J_2+J_3\ldots$	0.37, 0.40	0.21, 0.22
γ_{int}	$4(J_1+J_2+J_3\ldots)$	63, 63 (55)	26, 26 (22)
J_1		0.368	0.208
J_2		0.007	0.003
J_3		0.027	0.008

Ashcroft [34] has suggested that a Hume-Rothery argument, referring to the proximity of Brillouin-zone planes to the Fermi surface, could explain the special stability of the $9R$ phase in Li and hence by implication in other monovalent metals. The reasoning is based on the observation that the first Brillouin zone of the $9R$ structure is bounded by 38 planes, of which several are closer to the Fermi sphere than in bcc. A further investigation will examine the validity of this argument, which appears to be incompatible with our stacking-fault description of the energies of all the polytypes.

In summary, we have done computer simulations using empirical N-body potentials of the $\Sigma 3\langle 110\rangle(211)$ twin boundary in Ag. The simulations predict a 1-nm layer of $9R$ phase at the boundary. We have confirmed this prediction directly by HRTEM. We have calculated the energy of a perfect $9R$ structure and other polytypes from first-principles calculations and shown that they are well represented by a superposition of stacking-fault energies, the values of which are especially low in these metals. The occurrence of the broadened and faceted twin boundaries observed in Cu, Ag, and Au is now understood.

[1] S. Kajiwara and Z. Nishiyama, Jpn. J. Appl. Phys. **12**, 749 (1964).
[2] I. Cornelis and C. M. Wayman, Acta Metall. **22**, 291 (1974).
[3] J. Luyten and L. Delaey, Scr. Metall. **13**, 747 (1979).
[4] M. Fukamachi and S. Kajiwara, Jpn. J. Appl. Phys. **19**,

L479 (1980).
[5] A. Nagasawa and A. Tatsumi, Trans. Jpn. Inst. Met. **29**, 625 (1988).
[6] T. Tadaki and K. Shimizu, Trans. Jpn. Inst. Met. **18**, 735 (1977).
[7] Z. Zhang and Y.-k. Wu, Acta Phys. Sin. **33**, 696 (1984).
[8] J.-M. Dance and A. Tressaud, Mater. Res. Bull. **14**, 37 (1979).
[9] S. Kemmler-Sack and A. Ehmann, J. Solid State Chem. **44**, 366 (1982).
[10] C. De Blasi, A. M. Mancini, D. Manno, A. Rizzo, and E. Carlino, Nuovo Cimento **13D**, 233 (1991).
[11] S. Kajiwara, S. Ohno, K. Honma, and M. Uda, Philos. Mag. Lett. **55**, 215 (1987).
[12] P. J. Othen, M. L. Jenkins, G. D. W. Smith, and W. J. Phythian, Philos. Mag. Lett. **64**, 383 (1991).
[13] A. W. Overhauser, Phys. Rev. Lett. **53**, 64 (1984).
[14] C. M. McCartley, C. W. Thompson, and S. A. Werner, Phys. Rev. B **22**, 574 (1980).
[15] H. G. Smith, Phys. Rev. Lett. **58**, 1228 (1987).
[16] R. Berliner, O. Fajen, H. G. Smith, and R. L. Hitterman, Phys. Rev. B **40**, 12086 (1989).
[17] J. A. Wilson and M. de Podestal, J. Phys. F **16**, L121 (1986).
[18] T. W. Barbee, III and M. L. Cohen, Phys. Rev. B **43**, 5269 (1991).
[19] U. Wolf, F. Ernst, T. Muschik, M. W. Finnis, and H. F. Fischmeister, Philos. Mag. (to be published).
[20] U. Wolf, P. Gumbsch, H. Ichinose, and H. F. Fischmeister, J. Phys. Colloq. **51**, C1-359 (1990).
[21] G. S. Zhdanov, C. R. Acad. Sci. USSR **48**, 43 (1945).
[22] R. Cheng, R. J. Needs, and V. Heine, J. Phys. C **21**, 1049 (1988).
[23] J. J. A. Shaw and V. Heine, J. Phys. Condens. Matter **2**, 4351 (1990).
[24] G. J. Ackland, G. Tichy, V. Vitek, and M. W. Finnis, Philos. Mag. A **56**, 735 (1987).
[25] I. Sommer, C. Herzig, S. Mayer, and W. Gust, Defect Diffus. Forum **66–69**, 843 (1989).
[26] D. van Dyck, G. van Tendeloo, and S. Amelinckx, Ultramicroscopy **10**, 263 (1982).
[27] P. A. Stadelman, Ultramicroscopy **21**, 131 (1987).
[28] P. J. H. Denteneer and J. M. Soler, Solid State Commun. **78**, 857 (1991).
[29] D. G. Pettifor and C. Varma, J. Phys. C **12**, L253 (1979).
[30] A. R. Mackintosh and O. K. Andersen, *Electrons at the Fermi Surface* (Cambridge Univ. Press, New York, 1980).
[31] O. K. Andersen, Phys. Rev. B **12**, 3060 (1975).
[32] H. L. Skriver, *The LMTO Method* (Springer, Heidelberg, 1983).
[33] H. L. Skriver, Phys. Rev. B **31**, 1909 (1985).
[34] N. W. Ashcroft, Phys. Rev. B **39**, 10552 (1989).
[35] P. C. J. Gallagher, Metall. Trans. **1**, 2429 (1970).

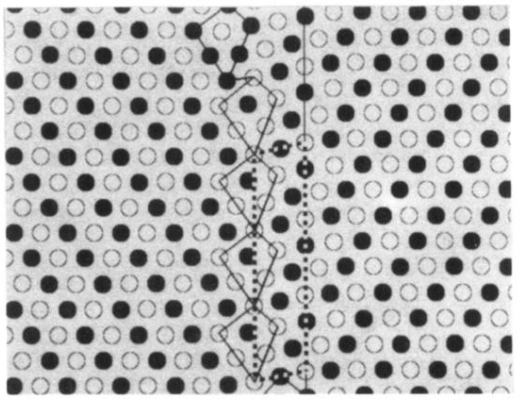

FIG. 1. A piece of the grain boundary in Ag simulated with molecular dynamics after annealing at 500 K for 20 ps followed by quenching.

FIG. 2. The (a) observed and (b) simulated HRTEM images of the grain boundary in Ag. (c) The atomic coordinates (x,y) extracted from (a) and used for the simulation (b). The black and white shading is our assignment of atoms to one of the two (220) planes in the z direction.